

Color Fundus Image Guided Artery-Vein Differentiation in Optical Coherence Tomography Angiography

Minhaj Alam,¹ Devrim Toslak,^{1,2} Jennifer I. Lim,³ and Xincheng Yao^{1,3}

¹Department of Bioengineering, University of Illinois at Chicago, Chicago, Illinois, United States

²Department of Ophthalmology, Antalya Training and Research Hospital, Antalya, Turkey

³Department of Ophthalmology and Visual Sciences, University of Illinois at Chicago, Chicago, Illinois, United States

Correspondence: Xincheng Yao, Department of Bioengineering (MC 563), University of Illinois at Chicago (UIC), Clinical Sciences North, Suite W103, Room 164D, 820 South Wood Street, Chicago, IL 60612, USA; xcy@uic.edu.

Jennifer I. Lim, Illinois Eye and Ear Infirmary, University of Illinois at Chicago, 1855 W. Taylor Street, Suite 2.50, M/C 648, Chicago, IL 60612, USA; jennyylim@uic.edu.

Submitted: May 18, 2018

Accepted: September 4, 2018

Citation: Alam M, Toslak D, Lim JI, Yao X. Color fundus image guided artery-vein differentiation in optical coherence tomography angiography. *Invest Ophthalmol Vis Sci.* 2018;59:4953-4962. <https://doi.org/10.1167/iovs.18-24831>

PURPOSE. This study aimed to develop a method for automated artery-vein classification in optical coherence tomography angiography (OCTA), and to verify that differential artery-vein analysis can improve the sensitivity of OCTA detection and staging of diabetic retinopathy (DR).

METHODS. For each patient, the color fundus image was used to guide the artery-vein differentiation in the OCTA image. Traditional mean blood vessel caliber (m-BVC) and mean blood vessel tortuosity (m-BVT) in OCTA images were quantified for control and DR groups. Artery BVC (a-BVC), vein BVC (v-BVC), artery BVT (a-BVT), and vein BVT (v-BVT) were calculated, and then the artery-vein ratio (AVR) of BVC (AVR-BVC) and AVR of BVT (AVR-BVT) were quantified for comparative analysis. Sensitivity, specificity, and accuracy were used as performance metrics of artery-vein classification. One-way, multilabel ANOVA with Bonferroni's test and Student's *t*-test were employed for statistical analysis.

RESULTS. Forty eyes of 20 control subjects and 80 eyes of 48 NPDR patients (18 mild, 16 moderate, and 14 severe NPDR) were evaluated in this study. The color fundus image-guided artery-vein differentiation reliably identified individual arteries and veins in OCTA. AVR-BVC and AVR-BVT provided significant ($P < 0.001$) and moderate ($P < 0.05$) improvements, respectively, in detecting and classifying NPDR stages, compared with traditional m-BVC analysis.

CONCLUSIONS. Color fundus image-guided artery-vein classification provides a feasible method to differentiate arteries and veins in OCTA. Differential artery-vein analysis can improve the sensitivity of OCTA detection and classification of DR. AVR-BVC is the most-sensitive feature, which can classify control and mild NPDR, providing a quantitative biomarker for objective detection of early DR.

Keywords: optical coherence tomography, diabetic retinopathy, image analysis, retina

Diabetic retinopathy (DR)¹⁻⁵ is a leading cause of preventable blindness worldwide. It is estimated that 40% to 45% diabetic patients can be affected by DR⁶ (~180 million people). Early detection and prompt treatment are essential to prevent DR-associated vision loss. DR is characterized by retinal vascular abnormalities, such as microaneurysms, exudates, arterial narrowing, venous beading, cotton wool spots, and so on.⁷ Quantitative imaging of retinal vasculature is important for DR diagnosis and treatment evaluation. Fundus photography has been traditionally used for quantitative assessment of retinal vasculature. However, fundus images cannot provide necessary sensitivity to reveal microvascular abnormality, which can be affected at early stage of DR.⁸ Especially the vasculature, including small capillaries and their associated distortions in the parafoveal region of the retina cannot be captured with fundus photography.⁹⁻¹¹ Fluorescein angiography (FA) can be used to improve imaging sensitivity of retinal vascular distortions in DR.^{12,13} However, FA requires intravenous dye injections, which may produce side effects and require careful management professionally.

Optical coherence tomography (OCT) can be used to identify morphologic changes at individual functional layers

of the retina and has increasing applications in eye disease detection and treatment evaluation.¹⁴ OCT angiography (OCTA) provides additional power to enable noninvasive observation of retinal vascular changes with spatial resolution at the individual capillary level.¹⁵ It allows depth-resolved visualization of multiple layers of the retina with high resolution, and can be more sensitive than traditional FA in detecting microvascular changes in retinal diseases.¹⁶ OCTA has been extensively used to conduct quantitative assessment of retinal vasculature in disease conditions.¹⁶⁻²¹ Multiple OCTA features, such as blood vessel caliber (BVC), blood vessel tortuosity (BVT), vessel perimeter index (VPI), foveal avascular zone (FAZ) area, FAZ contour irregularity, and retinal vascular density, have also been developed for quantitative OCTA analysis and computer-aided classification of age-related macular degeneration (AMD),²² DR,²³ glaucoma,²⁴ and sickle cell retinopathy (SCR).^{15,25} However, differential artery-vein analysis, which may provide improved sensitivity of DR detection and treatment assessment, in OCTA is challenging.

It is known that different systematic diseases and their progressing stages could affect arteries and veins differently.

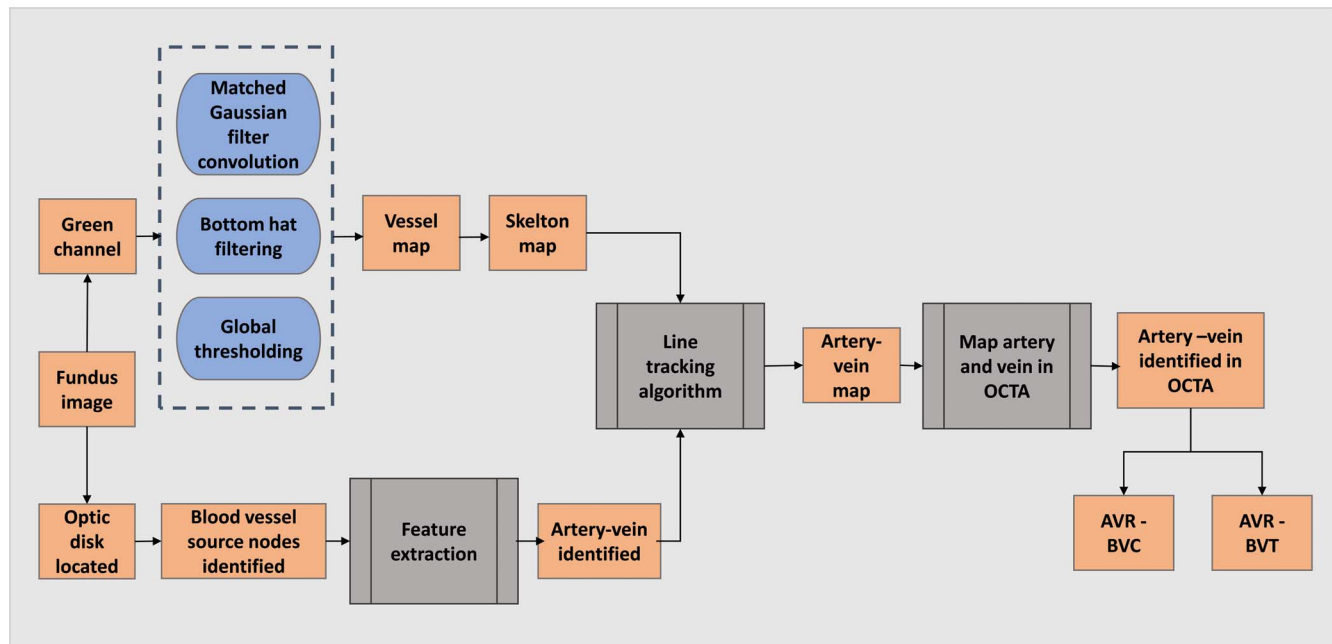


FIGURE 1. Flow diagram of the whole process.

Focal arterial narrowing^{26–28} and venous beading^{29–32} have been reported in patients with hypertension, diabetes, and other eye diseases. Artery-vein ratio (AVR) of calibers, for example, has been demonstrated as a predictor of these diseases,^{33–37} but only with fundus photo images. Currently, there are no established methods to differentiate arteries and veins in OCTA. Differential analysis of arteries and veins holds promise to improve the sensitivity of quantitative OCTA detection and classification of eye diseases. This project was designed to develop a method for quantitative analysis of arteries and veins in OCTA, and to verify that differential artery-vein analysis can improve the sensitivity of OCTA detection and classification of DR. We report here color fundus image-guided artery-vein differentiation as a feasible strategy to classify arteries and veins in OCTA. We also introduce AVR-BVC and AVR-BVT as two objective metrics for DR detection and classification.

METHODS

This section describes the methodology for quantitative analysis of OCTAs. Figure 1 illustrates the core steps of the OCTA data processing. The first step was fundus image-guided artery-vein classification of OCTA images and the second step was to measure and compare quantitative features for control and NPDR OCTA images.

Data Acquisition

This study was approved by the institutional review board of the University of Illinois at Chicago and followed the tenets of the Declaration of Helsinki. The DR patients were recruited from University of Illinois at Chicago retinal clinic. A retrospective study was conducted with 48 type II diabetic patients (18 mild, 16 moderate, and 14 severe NPDR) who underwent DR evaluation and fundus, OCT and OCTA imaging at retina clinic of University of Illinois at Chicago. All patients underwent a complete anterior and dilated posterior segment examination (JIL). The patients were classified by severity of

DR (mild, moderate, severe) according to the Early Treatment Diabetic Retinopathy Study (ETDRS) staging system by retina specialists using seven-fields fundus photographs. Control data were obtained from healthy volunteers who gave informed consent for fundus photography and OCTA imaging. We did not include subjects with history of other eye diseases, prior intravitreal injections, or previous vitreous surgery. The eyes with significant pathologic features, such as macular edema, vein occlusions, or epiretinal membranes, were excluded. Images of both eyes of every patient were acquired. All the images were qualitatively examined; fundus images with severe light saturation or uneven illumination in the parafoveal area were excluded. OCTA images with severe motion artifact were also excluded.

Color fundus images were captured using fundus cameras (Cirrus-800; Zeiss, Oberkochen, Germany; and Pictor by Volk nonmydriatic retinal camera; Volk Optical Inc., Mentor, OH, USA with a 30° to 45° field-of-view (FOV) and an image resolution of 2392 × 2048 pixels. Among the three channels of the fundus image (red, green, and blue), we used the green channel for blood vessel segmentation as it demonstrates the best contrast of the blood vessels.^{38–41} Several preprocessing steps, such as intensity, contrast adjustments, and normalization along with median filtering to remove noises, were performed before blood vessel segmentation in the fundus images.

Spectral-domain (SD)-OCT and OCTA images were acquired using an Angiovue SD-OCT angiography system (Optovue, Fremont, CA, USA), consisting of a 70-KHz A-scan rate, and axial and lateral resolutions of approximately 5 and 15 μm, respectively. All analyzed OCTA images were 6 × 6-mm scans. We only used OCTA images from superficial layer, which includes 80% of ganglion cell complex, containing all structures of inner plexiform layer up to the border with the inner nuclear layer. The issue with projection artifact was not significant in the superficial layer. The segmentation of the superficial layer was conducted in the commercially available software interface of Angiovue SD-OCT system (ReVue, Fremont, CA, USA).

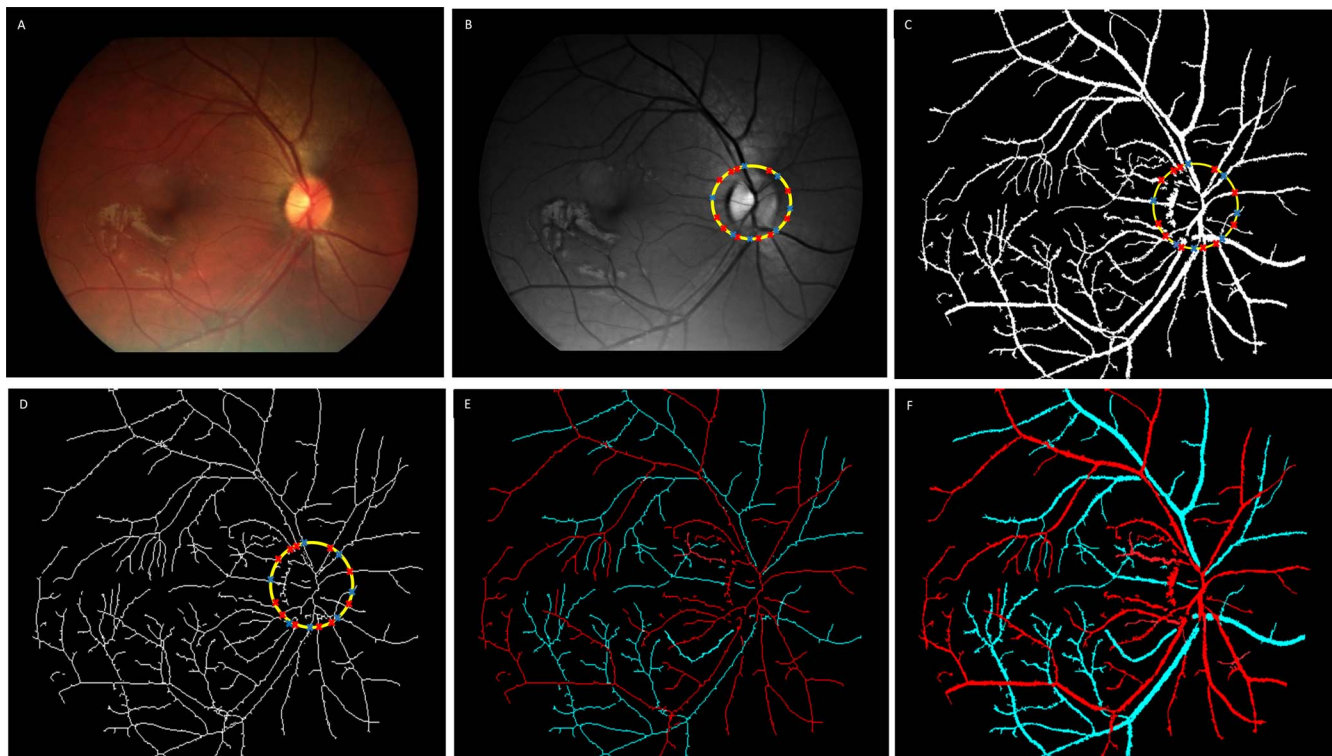


FIGURE 2. (A) Original fundus image. (B) Enhanced green channel image. Optic disc region located with *yellow circle* and artery-vein source nodes identified with *red and blue crosses*, respectively. (C) Segmented vessel map. (D) Skeleton map. (E) Artery-vein identified in skeleton map. (F) Artery-vein map.

We exported the fundus and OCTA images, and used custom-developed MATLAB (Mathworks, Natick, MA, USA) procedures with graphic user interface for further image analysis, feature extraction, and image classification as described below.

Artery-Vein Classification in Fundus Images

We combined optical density ratio (ODR) analysis and blood vessel tracking algorithm to identify artery-vein in color fundus images (Fig. 2A). Technical details of the fully automated artery-vein classification algorithm have been reported in our recent publication.⁴² For this procedure, we used a matched-filtering method-based blood vessel-enhancing technique^{42,43} (Fig. 2B) on the green channel image and segmented the blood vessel map (Fig. 2C) and skeleton map (Fig. 2D). The segmented blood vessel map and ODR analysis around the optic disc are used to determine the blood vessel source nodes. The whole vessel map is then tracked beginning from the source nodes using vessel curvature-angle information and classified as vein (venule) or artery (arteriole; Figs. 2E, 2F).

Artery Vein Mapping in OCTA

We used the artery-vein map derived from color fundus image to classify arteries and veins in OCTA image. OCTA covers parafoveal vascular structures; while color fundus image covers a larger field of view covering the perifoveal area of the retina and optic disc. Therefore, we can map the blood vessels of parafoveal region of color fundus image on to OCTA images. We employed an algorithm, which overlays the OCTA and fundus image parafoveal regions, based on foveal center coordinates, and then uses image registration to align the blood vessels.

We selected a foveal candidate region that had the darkest intensity values⁴⁴ and was located temporal to the optic disc and within the elliptical main vascular arches.⁴⁵ Figure 3A illustrate representative image with identified foveal location and its center pixel is marked by a green window with a red cross in the center of the fovea. Upon selecting the foveal center coordinate, we chose a parafoveal region of interest (PROI; green dashed square, Fig. 3A), which was used for image registration and mapping of artery-vein vessels to OCTA. For the OCTA image, the field of view was a square 6×6 -mm parafoveal region and the fovea center was identified at the center coordinate of the image (Fig. 3B). For further image registration, we used the binarized vessel map of the OCTA (Fig. 3C). For the OCTA vessel map, we used a Hessian based multiscale Frangi filter⁴⁶ to enhance the vascular flow information. Frangi filtering method uses the Eigen vectors of the Hessian matrices and computes the likeliness of a OCTA region to be vascular structures. Adaptive thresholding and morphologic functions were further used for cleaning the vessel map and removing small capillary mesh structures that were not feasible for vessel tracking algorithm. The extracted vessel maps from OCTA images had an average area of 17.80% (SD: 3.4, range: 14%–22%).

After locating the fovea centers on both fundus and OCTA images, the OCTA vessel map was overlaid on the PROI by overlapping the center coordinates (Fig. 3D). At this point, the images were overlaid but the vessel structures were not properly registered. We used a geometric-affine image registration method⁴⁷ for recursive alignment of the binarized PROI and OCTA vessel map, the example of a final result after image registration is shown in Figure 3E. The image registration method employed a geometric deformation model, which was a global affine transformation combined

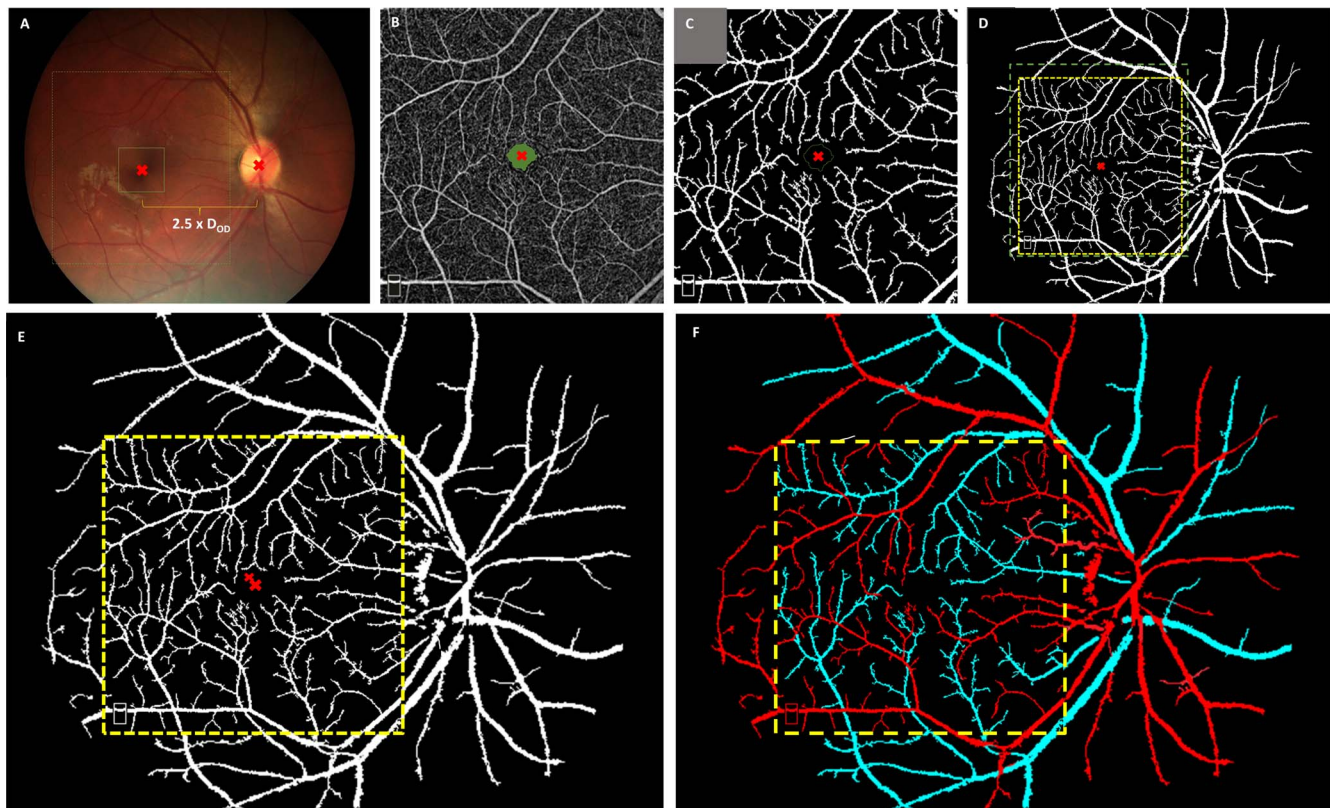


FIGURE 3. (A) Optic disc and fovea identified in original fundus image; the center pixels are identified with *red crosses*. (B) Corresponding OCTA image with fovea and its center identified. (C) Segmented vessel map from OCTA. (D) Vessel map from fundus and OCTA images mapped based on center coordinate of the fovea. (E) OCTA mapped into fundus after image registration. (F) Artery-vein mapped on OCTA image.

with isometric scaling method.⁴⁷ The overall artery-vein mapping process including overlapping of center coordinates and image registration of the binary PROI and OCTA vessel maps were automatically performed using MATLAB and ImageJ software (<http://imagej.nih.gov/ij/>; provided in the public domain by the National Institutes of Health, Bethesda, MD, USA).

Upon registration, the artery-vein classification of fundus image was mapped onto the OCTA image. If the OCTA had additional vascular branches, they were tracked back to the source nodes and classified as artery or vein accordingly.⁴² Skeleton vessel maps were used for the vessel tracking. Before tracking, morphologic closing function and noise filtering were used on the skeleton maps to remove any remaining noises and spur pixels. Each of the endpoints and branchpoints of the additional vessel branches in the skeleton map were identified automatically using morphologic functions in MATLAB. The endpoints were linked with the already identified (artery or vein) source nodes using a blood vessel tracking technique that employs ODR, textural, and morphologic features. This vessel-tracking algorithm also involves protocol for intersections (2-, 3-, or 4-way), gaps in the tracking path and vessel overlapping. Further detail of the tracking algorithm can be found in our recent publication.⁴² The performance of the automated artery-vein classification in fundus and OCTA images were validated with ground truths prepared by two independent graders (JIL and DT). The ground truths only referred to vessel areas with identical artery-vein assignments by these two independent graders.

Quantitative Analysis of OCTA

Using the color fundus image-guided artery-vein classification of all the OCTA images, we conducted the quantitative analysis for control and NPDR stages. From the artery-vein OCTA map (Fig. 4A), we obtained skeletonized artery-vein maps (Fig. 4B) and corresponding artery and vein maps (Figs. 4C, 4D). Traditional m-BVC and m-BVT without artery-vein differentiation in OCTA were first quantified for control and NPDR groups. Then, artery BVC (a-BVC), vein BVC (v-BVC), artery BVT (a-BVT), and vein BVT (v-BVT) were quantified for comparisons studies. AVR-BVC and AVR-BVT were calculated based on corresponding a-BVC, a-BVT and v-BVC, v-BVT, respectively.

For measuring the BVC (artery or vein), we used both the vessel and skeleton map. The average BVC (m-BVC) can be defined as the ratio of the vascular area (calculated from vessel map) and vascular length (calculated from the skeleton map).¹⁵ For a-BVC and v-BVC, we used corresponding artery and vein vessel and skeleton maps. AVR-BVC was calculated from a-BVC and v-BVC, defined as,

$$AVR-BVC = \frac{\text{Mean arterial BVC}}{\text{Mean venous BVC}} \quad (1)$$

In case of BVT, each branch of vessel capillaries was identified with two endpoints (one example is illustrated in Fig. 4C, X and Y denote two such endpoints) in the skeleton map. BVT of a single vessel branch can be calculated using the distance metric,^{15,48,49} which is a ratio of geodesic distance and Euclidian distance between two endpoints of a vessel branch. Geodesic distance represents the curve length (real length) while Euclidian distance represents the imaginary straight

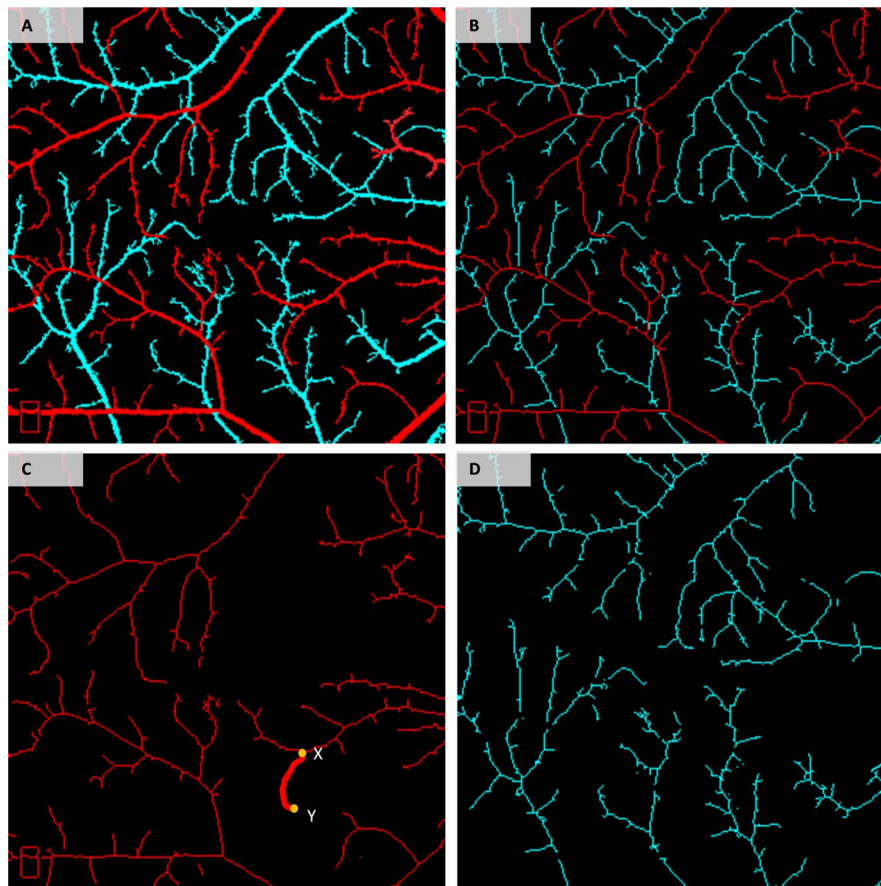


FIGURE 4. (A) Artery-vein map in OCTA. (B) Artery-vein skeleton map in OCTA. (C) Artery-skeleton map. (D) Vein-skeleton map.

length between two endpoints. We calculate the BVT for each separate vessel branches and measure the average BVT for a single OCTA image (m-BVT).¹⁵ Corresponding a-BVT and v-BVT were measured from artery and vein skeleton maps. AVR-BVT was measured then as,

$$AVR-BVT = \frac{\text{Mean arterial BVT}}{\text{Mean venous BVT}} \quad (2)$$

Statistical Analyses

We conducted all the statistical analyses using MATLAB and OriginPro (OriginLab Corporation, Northampton, MA, USA). We employed a one-way, multilabel ANOVA with Bonferroni's test to compare difference of the mean values of these vascular parameters among multiple groups. One versus one comparisons of these parameters between the control and NPDR (mild/moderate/severe) stages were performed by the two-sample paired Student's *t*-test. We used χ^2 test was used to compare the distribution of sex and hypertension among different groups, age distribution was compared using ANOVA. The repeatability of AVR-BVC and AVR-BVT features were tested using intraclass correlation coefficients (ICC) from two-repeat measurements. For all measurements, statistical significance was defined as $P < 0.05$.

RESULTS

Images from 40 eyes of 20 control subjects and 80 eyes of 48 NPDR patients (18 mild, 16 moderate, and 14 severe NPDR)

were used for this study. The database consisted of 40 control, 30 mild NPDR, 27 moderate NPDR, and 23 severe NPDR images. The detailed patient demographic data are shown in the Table. There were no statistically significant differences between control and NPDR groups with respect to age, sex, or hypertension distribution (ANOVA, $P = 0.19$; χ^2 test, $P = 0.24$ and $P = 0.22$, respectively).

The automated artery-vein classification in both fundus and OCTA images were validated using ground truths manually labeled by two retina specialists (JIL and DT). There were 96.21% and 93.97% agreements between the two observers on the identified artery-vein vessel maps for the fundus and OCTA images, respectively. This indicates that these 96.21% and 93.97% vessel areas can be used as the ground truths to validate the performance of automated artery-vein classification in fundus and OCTA images, respectively. As the artery-vein classification was performed on the extracted binarized vessel maps in fundus and OCTA images, the manual labeling was also prepared using the vessel maps so that there was consistency in the prepared ground truths and identified artery-vein maps. The smallest parafoveal capillaries in the OCTA images were not included in the vessel map and were also excluded from the manual labeling. For the fundus images, we used a matched filtering-based robust vessel-enhancing technique, which enabled robust segmentation of the vessel map with intricate details. We observed an average of 21% increase in the vasculature map in fundus images compared with the original one without vessel enhancement. For each of the ground truth images (both fundus and OCTA), the observers manually traced the whole binary vessel map with blue (for veins) and red (for arteries) markings and identified

TABLE. Demographics of Control and DR Subjects

	Control	Diabetic Retinopathy		
		Mild NPDR	Moderate NPDR	Severe NPDR
Number of subjects	20	18	16	14
Number of images	40	30	27	23
Sex (male/female)	12/8	11/7	10/6	6/8
Age (mean \pm SD), y	42 \pm 9.8	52.2 \pm 10.24	48.5 \pm 7.29	53.33 \pm 5.71
Age, range, y	25-71	24-73	36-68	45-73
Duration of diabetes, (mean \pm SD), y	-	14.75 \pm 9.48	12.56 \pm 9.48	17.80 \pm 10.43
HTN prevalence, %	10	72.22	68.75	85.71

HTN, hypertension.

the branchpoints with yellow markings. Each of the manually identified nodes and artery-vein branches were matched pixel-wise with the classification results to measure the performance metrics. If the two graders had disagreement on specific areas of the vessel map, that area was labeled as unclassified and excluded from the ground truth. For evaluating the classification performance on all fundus and OCTA images (control and NPDR patients), sensitivity, specificity, and accuracy metrics were measured. The algorithm demonstrated 98.51% and 98.26% accuracies in identifying blood vessels as artery and vein, respectively, in the fundus images (ICC 0.98 and 0.96 for two-repeat measurement, 95% CI 0.91-1). There was 98.64% sensitivity and 96.13% specificity for artery identification and 98.36% sensitivity and 95.97% specificity for vein identification. For OCTA images, we observed 97.29% sensitivity and 96.57% specificity for artery identification and 97.38% sensitivity and 96.14% specificity for vein identification. The accuracies were 97.03% and 97.24%, respectively, for identifying blood vessels as artery and vein in the OCTA images (ICC 0.95 and 0.94 for two-repeat measurement, 95% CI 0.88-0.97). These performance metrics indicate that the automated classification performs really well for robust identification of arteries and veins, compared with manually labeled ground truths.

Quantitative analysis of control and NPDR OCTAs is summarized in Figures 5A and 5B. The AVR-BVC and AVR-

BVT features demonstrated excellent repeatability with two-repeat measurement. The corresponding ICC and 95% CIs for AVR-BVC and AVR-BVT are 0.97 (CI: 0.96-10) and 0.94 (CI: 0.89-0.94), respectively. We compare the sensitivity of AVR-BVC and AVR-BVT with m-BVC and m-BVT, respectively. We also verified if AVR-BVC and AVR-BVT improved the feature sensitivity for control versus NPDR OCTAs compared with a-BVC, a-BVT or v-BVC, v-BVT. For BVC analysis, although m-BVC increased slightly as NPDR stage progressed, it was not statistically significant. We observed 0.72%, 2.54%, and 4.04% increase for mild, moderate, and severe NPDR, compared with control data. For a-BVC and v-BVC analyses, 9.44%, 16.39%, and 24.59% decreases and 10.63%, 20.9%, and 31.95% increases were observed for control versus mild, control versus moderate, and control versus severe NPDR OCTAs, respectively. Because of the opposite polarity of a-BVC and v-BVC, the m-BVC change was not statistically significant. However, in case of AVR-BVC, the opposite polarities of a-BVC and v-BVC result in enhanced sensitivity in different NPDR stages. Compared with control OCTA data 18.14%, 30.9%, and 42.85% decreases were observed for mild, moderate, and severe NPDR OCTAs (Student's *t*-test, $P < 0.001$ for all three cases). The AVR-BVC change was also significant among the four groups (control and three NPDR groups; ANOVA, $P = 0.004$). In contrast, a-BVC, v-BVC, or mean BVC differences were not significant among the four groups. AVR-BVC was the best feature to differentiate

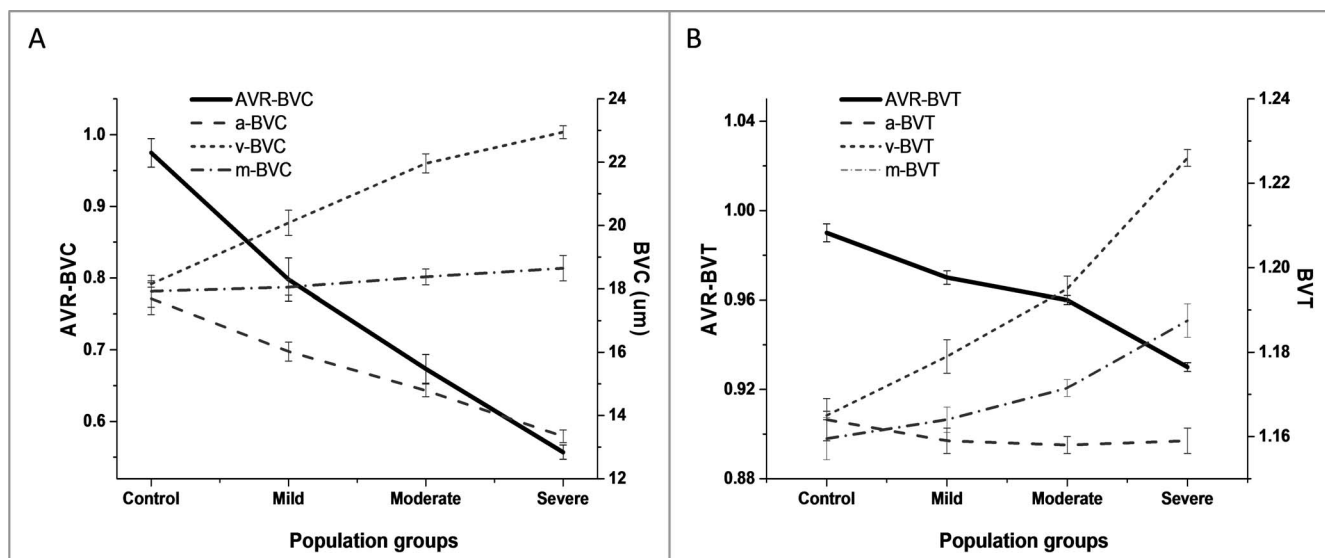


FIGURE 5. (A) BVC changes between control and NPDR patients. The unit (y axis on right) for a-BVC, v-BVC, m-BVC is micrometers; AVR-BVC is a ratio of a-BVC and v-BVC (y axis in left). (B) BVT changes between control and NPDR patients. BVT (y axis on right) is a ratio of geodesic and Euclidian distance. AVR-BVT is a ratio of a-BVT and v-BVT (y axis on left).

control from mild NPDR using OCTA (Student's *t*-test, $P < 0.001$), promising a unique biomarker for detecting early onset of NPDR in diabetes patients.

For BVT analysis, AVR-BVT improved the sensitivity, compared with m-BVT, but was not as significant as AVR-BVC. The a-BVT demonstrated minute changes between control and NPDR groups, but v-BVT increased as NPDR stage progressed. For v-BVT, 1.19%, 2.5%, and 5.1% increases were observed for control versus mild NPDR (not significant), control versus moderate NPDR (moderately significant, $P < 0.05$), and control versus severe NPDR (moderately significant, $P < 0.05$) OCTA. Intergroup change in v-BVT was also not statistically significant (ANOVA, $P = 0.75$). The m-BVT demonstrated limited change in control and NPDR groups (0.38%, 1.03%, and 2.39% increases in mild, moderate, and severe NPDR groups compared with control). For AVR-BVT, 1.6%, 3%, and 5.4% decreases were observed for control versus mild, control versus moderate, and control versus severe NPDR (moderately significant, $P < 0.05$ for all cases) eyes. It could distinguish between mild and severe NPDR (Student's *t*-test, $P = 0.038$). However, AVR-BVT could not differentiate mild and moderate NPDR groups with statistical significance (Student's *t*-test, $P = 0.28$). Intergroup change in AVR-BVT was also not statistically significant (ANOVA, $P = 0.092$).

DISCUSSION

This study demonstrated that automated artery-vein differentiation in OCTA is possible using blood vessel tracking from color fundus images. The algorithm facilitated a feasible method to differentiate individual arteries or veins in OCTA images (97.03% and 97.24% accuracies, respectively). In addition, the algorithm provided a means to differentiate and quantify changes in artery and vein, between control eyes and DR eyes. As artery and vein diameter and tortuosity can be affected in different way by DR, the differential artery-vein analysis improved the performance of quantitative OCTA features. Due to opposite polarities of a-BVC and v-BVC (i.e., arterial narrowing and venous widening) in DR patients, m-BVC did not reveal significant differences among control and DR groups. In contrast, the AVR-BVC provided excellent sensitivity to differentiate the control and NPDR stages. AVR-BVT also enhanced the sensitivity, but was not comparable to AVR-BVC performance. AVR-BVC was the most sensitive feature to reliably differentiate control and mild NPDR OCTAs promising a unique biomarker for early detection of mild NPDR.

There has been a widespread interest in artery-vein classification among researchers, which can be directly linked to its potential applications in clinical assessments. With robust and accurate identification of arteries and vein, subtle microvascular distortions in retina could be analyzed for different systematic and ocular diseases. However, most studies have used fundus images to attempt artery-vein classification vein⁵⁰⁻⁵⁶ as it provides color, intensity, and contrast information that is often crucial to differentiate arteries and veins. Most of the algorithms based on fundus images rely on the intensity and color information of artery and vein.⁵⁰⁻⁵⁶ Researchers have also explored semiautomatic algorithms⁵⁷⁻⁵⁹ using supervised classification and incorporated functional features like ODR to identify artery and vein in fundus images.⁶⁰⁻⁶² We recently demonstrated an artery-vein classification algorithm incorporating ODR and vessel tracking that showed excellent performance in identifying artery-vein in fundus images⁴² compared with recent artery-vein classification algorithms⁶³⁻⁶⁵ (97.06% accuracy using 50 fundus images compared to 92%, 90.08%, and 88.28%, respectively). Employing a robust vessel

enhancing technique improved the overall extracted blood vessel map and enabled swift vessel tracking. The blood vessel tracking algorithm also had protocols for intersections, four-way crossovers, and gaps in the skeleton map, further details can be found in our published article.⁴²

Robust artery-vein classification in fundus image has been well established. However, to the best of our knowledge, there has been no reported attempt for artery-vein identification in OCTA images. As OCTA provides high-resolution flow information near fovea and excellent spatial resolution at individual capillary plexuses, it has been recently explored as an excellent quantitative imaging platform. Several features have showed effectiveness in quantifying microvascular distortions caused by DR,²³ AMD,²² DR,²³ glaucoma,²⁴ SCR.^{15,25} and so on in OCTA images. Quantifying these features differentially in artery and vein hold potential of increased sensitivity, especially for early detection of the retinal diseases. We report a feasible strategy in this pilot study to differentiate artery and vein in OCTA. This algorithm employs a fundus image-guided artery-vein classification strategy and maps the artery-vein information from fundus image to the corresponding OCTA image. This is done by locating the fovea in both fundus and OCTA images and then using a geometric-affine image registration method for recursive alignment of binarized OCTA vessel map and fundus image parafoveal region. The image registration was crucial to enable transfer of the artery-vein information from fundus image vessel map to OCTA vessel map. It was a global affine transformation model combined with isometric scaling method and was robust for binarized input images. Each of the fundus image PROI-OCTA map overlay was qualitatively examined by two trained ophthalmologists and the identified artery-vein maps in OCTA images were further validated with the labeled ground truths prepared by them. The automated artery-vein classification was applied to the full retinal area for differential artery-vein analysis. However, only the blood vessels on which the two graders had an agreement on artery-vein assignment were selected to verify the performance of the automated artery-vein classification.

Another major part of the artery-vein classification process is the blood vessel tracking algorithm that is largely dependent on the extracted vessel map from both fundus and OCTA images. Generally, there should be alternative positioning of artery and vein around optic nerve head (ONH). However, the presence of cilioretinal artery and multiple branches coming out of the central retinal artery may increase the number of arteries in the temporal area. In a smaller radius around ONH, the artery-vein ratio is close to 1:1. Imaging related issues like this vary with different subjects and corresponding fundus image quality. To reduce the effect on the overall performance, we maintained a general standard for all the included fundus images in our study. The images that did not clearly show the optic disk and foveal area in the retina were excluded. Approximately 11% images from the total database had to be excluded for various quality control issues (120 from 136 were used). The matched-filtering technique for vessel enhancement-enabled vessel map extraction even from blurred fundus images. However, severely blurred images with significantly low contrast to noise ratio (CNR) were excluded. The artery-vein classification in fundus images failed if the vascular structures in the parafoveal area could not be extracted properly. However, the vessel-tracking algorithm was robust and worked even in case of gaps in vessel skeleton. The tracking adaptively increased its pixel-searching window if it came upon a gap in vessel skeleton. For OCTAs, similar qualitative inclusion criteria were maintained and images with severe motion artifact were excluded. The Frangi filtering enabled decent segmentation of vessel maps but some images needed intensity normalization and contrast adjustment prior

to vessel segmentation. As we only used superficial layer for OCTA imaging, the projection artifact was not a significant issue as they mainly occur in OCTAs from deeper retinal layers. However, the tracking failed in the smallest capillary mesh structures in the parafoveal area, so we excluded them from the extracted vessel maps. The 3×3 -mm OCTA scans provide higher resolution in the parafoveal area. In our future study, we plan to use the higher resolution 3-mm FOV OCTAs for vessel tracking and classify the small capillary structures into artery and veins.

Our preliminary study confirms the importance of differential artery-vein analysis in OCTA. Further investigation with a much larger population could yield in better performance for DR detection and classification. In addition, the database only used OCTAs from single device in a single-academic center. Future studies would include larger datasets, combined OCTAs taken from different OCT manufacturers, and use a validation OCTA dataset from other institutions. For the artery-vein classification, it can be interesting to further implement multifeature techniques with functional and structural features, such as ODR, vessel dimension, shape, curvature, intensity-contrast information, and so on. Employing deep-convolutional networks for unsupervised classification might also yield better artery-vein classification performance in both fundus and OCTA images. Alternative to fundus imaging, Doppler OCT can also be useful in guided artery-vein identification in OCTA images.

In conclusion, color fundus image-guided artery-vein classification provides a feasible method to differentiate arteries and veins in OCTA. Two objective OCTA features (i.e., AVR-BVC and AVR-BVT) enabled objective and differential analysis of arteries and veins to improve the sensitivity of OCTA detection and classification of DR. AVR-BVC is the most sensitive feature, which can reliably classify control and mild NPDR OCTAs. These findings will be useful in the development of automated machine-guided screening for detection of DR.

Acknowledgments

Supported in part by National Institutes of Health Grants R01 EY023522, R01 EY024628, P30 EY001792 (Bethesda, MD, USA), by an unrestricted grant from Research to Prevent Blindness (New York, NY, USA), by a Richard and Loan Hill endowment (Chicago, IL, USA), and by a Marion H. Schenk Chair endowment (Chicago, IL, USA).

Disclosure: **M. Alam**, P; **D. Toslak**, None; **J.I. Lim**, None; **X. Yao**, P

References

1. Stanga PE, Boyd SR, Hamilton AM. Ocular manifestations of diabetes mellitus. *Curr Opin Ophthalmol*. 1999;10:483-489.
2. Akil H, Bulus AD, Andiran N, Alp MN. Ocular manifestations of type 1 diabetes mellitus in pediatric population. *Indian J Ophthalmol*. 2016;64:654-658.
3. Milkie GM. Ocular manifestations associated with diabetes mellitus; a case report. *Am J Optom Arch Am Acad Optom*. 1956;33:604-608.
4. Saclarides TJ. Diabetes mellitus: classification, etiology, diagnosis, complications, and possible ocular manifestations. *J Ophthalmic Nurs Technol*. 1982;1:33-39, 50.
5. Wilkinson CP, Ferris FL, Klein RE, et al. Proposed international clinical diabetic retinopathy and diabetic macular edema disease severity scales. *Ophthalmology*. 2003;110:1677-1682.
6. International Diabetes Federation (IDF). IDF Diabetes Atlas 7th edition; 2015. Available at: <http://www.diabetesatlas.org/>. Accessed October 20, 2016.
7. Nayak J, Bhat PS, Acharya UR, Lim CM, Kagathi M. Automated identification of diabetic retinopathy stages using digital fundus images. *J Med Syst*. 2008;32:107-115.
8. Zahid S, Dolz-Marco R, Freund KB, et al. Fractal dimensional analysis of optical coherence tomography angiography in eyes with diabetic retinopathy. *Invest Ophthalmol Vis Sci*. 2016; 57:4940-4947.
9. Gramatikov BI. Modern technologies for retinal scanning and imaging: an introduction for the biomedical engineer. *Biomed Eng Online*. 2014;13:52.
10. Mendis KR, Balaratnasingam C, Yu P, et al. Correlation of histologic and clinical images to determine the diagnostic value of fluorescein angiography for studying retinal capillary detail. *Invest Ophthalmol Vis Sci*. 2010;51:5864-5869.
11. Cheng S-C, Huang Y-M. A novel approach to diagnose diabetes based on the fractal characteristics of retinal images. *IEEE Trans Inform Technol Biomed*. 2003;7:163-170.
12. Gass JD. A fluorescein angiographic study of macular dysfunction secondary to retinal vascular disease. VI. X-ray irradiation, carotid artery occlusion, collagen vascular disease, and vitritis. *Arch Ophthalmol*. 1968;80:606-617.
13. Talu S, Calugaru DM, Lapascu CA. Characterisation of human non-proliferative diabetic retinopathy using the fractal analysis. *Int J Ophthalmol-Cbi*. 2015;8:770-776.
14. Goebel W, Kretzchmar-Gross T. Retinal thickness in diabetic retinopathy: a study using optical coherence tomography (OCT). *Retina*. 2002;22:759-767.
15. Alam M, Thapa D, Lim JI, Cao D, Yao X. Quantitative characteristics of sickle cell retinopathy in optical coherence tomography angiography. *Biomed Opt Express*. 2017;8:1741-1753.
16. Minvielle W, Caillaux V, Cohen SY, et al. Macular microangiopathy in Sickle cell disease using optical coherence tomography angiography. *Am J Ophthalmol*. 2016;164:137-144.
17. Lim JI. Ophthalmic manifestations of sickle cell disease: update of the latest findings. *Curr Opin Ophthalmol*. 2012; 23:533-536.
18. Hoang QV, Chau FY, Shahidi M, Lim JI. Central macular splaying and outer retinal thinning in asymptomatic sickle cell patients by spectral-domain optical coherence tomography. *Am J Ophthalmol*. 2011;151:990-994.e1.
19. Asdourian GK, Nagpal KC, Busse B, et al. Macular and perimacular vascular remodelling sickling haemoglobinopathies. *Br J Ophthalmol*. 1976;60:431-453.
20. Condon PI, Serjeant GR. Ocular findings in homozygous Sickle-cell anemia in Jamaica. *Am J Ophthalmol*. 1972;73: 533-543.
21. Ishibazawa A, Nagaoka T, Takahashi A, et al. Optical coherence tomography angiography in diabetic retinopathy: a prospective pilot study. *Am J Ophthalmol*. 2015;160:35-44.
22. Palejwala NV, Jia Y, Gao SS, et al. Detection of non-exudative choroidal neovascularization in age-related macular degeneration with optical coherence tomography angiography. *Retina (Philadelphia, Pa)*. 2015;35:2204.
23. Kim AY, Chu Z, Shahidzadeh A, Wang RK, Puliafito CA, Kashani AH. Quantifying microvascular density and morphology in diabetic retinopathy using spectral-domain optical coherence tomography angiography. *Invest Ophthalmol Vis Sci*. 2016;57:OCT362-OCT370.
24. Holló G. Vessel density calculated from OCT angiography in 3 peripapillary sectors in normal, ocular hypertensive, and glaucoma eyes. *Eur J Ophthalmol*. 2016;26:e42-e45.
25. Alam M, Thapa D, Lim JI, Cao D, Yao X. Computer-aided classification of sickle cell retinopathy using quantitative features in optical coherence tomography angiography. *Biomed Opt Express*. 2017;8:4206-4216.

26. Pedersen L, Jeppesen P, Knudsen ST, Poulsen PL, Bek T. Improvement of mild retinopathy in type 2 diabetic patients correlates with narrowing of retinal arterioles. A prospective observational study. *Graefes Arch Clin Exp Ophthalmol*. 2014;252:1561-1567.
27. Klein R, Klein BE, Moss SE, Wang Q. Hypertension and retinopathy, arteriolar narrowing, and arteriovenous nicking in a population. *Arch Ophthalmol*. 1994;112:92-98.
28. Cheung N, Bluemke DA, Klein R, et al. Retinal arteriolar narrowing and left ventricular remodeling: the multi-ethnic study of atherosclerosis. *J Am Coll Cardiol*. 2007;50:48-55.
29. Fonseca RA, Dantas MA. Retinal venous beading associated with recurrent branch vein occlusion. *Can J Ophthalmol*. 2002;37:182-183.
30. Gregson PH, Shen Z, Scott RC, Kozousek V. Automated grading of venous beading. *Comput Biomed Res*. 1995;28:291-304.
31. Kozousek V, Shen Z, Gregson P, Scott RC. Automated detection and quantification of venous beading using Fourier analysis. *Can J Ophthalmol*. 1992;27:288-294.
32. Piguet B, Gross-Jendroska M, Holz FG, Bird AC. Inherited venous beading. *Eye*. 1994;8(Pt 1):84-88.
33. Niemeijer M, Xu X, Dumitrescu AV, et al. Automated measurement of the arteriolar-to-venular width ratio in digital color fundus photographs. *IEEE Trans Med Imaging*. 2011;30:1941-1950.
34. Hubbard LD, Brothers RJ, King WN, et al. Methods for evaluation of retinal microvascular abnormalities associated with hypertension/sclerosis in the atherosclerosis risk in communities study. *Ophthalmology*. 1999;106:2269-2280.
35. Ikram MK, Witteman JC, Vingerling JR, Breteler MM, Hofman A, de Jong PT. Retinal vessel diameters and risk of hypertension. *Hypertension*. 2006;47:189-194.
36. Liew G, Wong TY, Mitchell P, Cheung N, Wang JJ. Retinopathy predicts coronary heart disease mortality. *Heart*. 2009;95:391-394.
37. Wong TY, Knudtson MD, Klein R, Klein BE, Meuer SM, Hubbard LD. Computer-assisted measurement of retinal vessel diameters in the Beaver Dam Eye Study: methodology, correlation between eyes, and effect of refractive errors. *Ophthalmology*. 2004;111:1183-1190.
38. Huang K, Yan M. A region based algorithm for vessel detection in retinal images. *Med Image Comput Comput Assist Interv*. 2006;9(Pt 1):645-653.
39. Walter T, Massin P, Erginay A, Ordonez R, Jeulin C, Klein J-C. Automatic detection of microaneurysms in color fundus images. *Medical Image Anal*. 2007;11:555-566.
40. Gharabaghi S, Daneshvar S, Sedaaghi MH. Retinal image registration using geometrical features. *J Digit Imaging*. 2013;26:248-258.
41. Daniel E, Anitha J. Optimum green plane masking for the contrast enhancement of retinal images using enhanced genetic algorithm. *Optik-International Journal for Light and Electron Optics*. 2015;126:1726-1730.
42. Alam M, Son T, Toslak D, Lim JI, Yao X. Combining optical density ratio and blood vessel tracking for automated artery-vein classification and quantitative analysis in color fundus images. *Trans Vis Sci Tech*. 2018;7(2):23.
43. Chaudhuri S, Chatterjee S, Katz N, Nelson M, Goldbaum M. Detection of blood vessels in retinal images using two-dimensional matched filters. *IEEE Trans Med Imaging*. 1989;8:263-269.
44. Abramoff M, Kay CN. Image processing. In: Ryan S, Schacht A, Wilkinson C, Hinton D, Sadda SV, Wiedemann P, eds. *Retina*. 5th ed: Elsevier Inc.; 2012:151-176.
45. Gegundez-Arias ME, Marin D, Bravo JM, Suero A. Locating the fovea center position in digital fundus images using thresholding and feature extraction techniques. *Comput Med Imaging Graph*. 2013;37:386-393.
46. Frangi AF, Niessen WJ, Vincken KL, Viergever MA. Multiscale vessel enhancement filtering. In: WM, Wells Colchester A, Delp S, eds. *International Conference on Medical Image Computing and Computer-Assisted Intervention*. Berlin: Springer; 1998:130-137.
47. Thevenaz P, Ruttimann UE, Unser M. A pyramid approach to subpixel registration based on intensity. *IEEE Trans Image Proc*. 1998;7:27-41.
48. Goldbaum MH. Retinal depression sign indicating a small retinal infarct. *Am J Ophthalmol*. 1978;86:45-55.
49. Hart WE, Goldbaum M, Cote B, Kube P, Nelson MR. Measurement and classification of retinal vascular tortuosity. *Int J Med Informatics*. 1999;53:239-252.
50. Grisan E, Ruggeri A. A divide et impera strategy for automatic classification of retinal vessels into arteries and veins. In: *Engineering in Medicine and Biology Society, 2003 Proceedings of the 25th Annual International Conference of the IEEE*. 2003:890-893.
51. Jelinek H, Depardieu C, Lucas C, Cornforth D, Huang W, Cree M. Towards vessel characterization in the vicinity of the optic disc in digital retinal images. *Image Vis Comput Conf*. 2005:2-7.
52. Li H, Hsu W, Lee M-L, Wang H. A piecewise Gaussian model for profiling and differentiating retinal vessels. In: *Image Processing, 2003 ICIP 2003 Proceedings 2003 International Conference of the IEEE*. 2003:1-1069.
53. Niemeijer M, van Ginneken B, Abramoff MD. Automatic classification of retinal vessels into arteries and veins. *Med Imaging*. 2009;72601:72601F.
54. Simó A, de Ves E. Segmentation of macular fluorescein angiographies. A statistical approach. *Pattern Recog*. 2001;34:795-809.
55. Vázquez S, Barreira N, Penedo M, Penas M, Pose-Reino A. Automatic classification of retinal vessels into arteries and veins. In: *7th International Conference Biomedical Engineering (BioMED 2010)*. 2010:230-236.
56. Vázquez S, Cancela B, Barreira N, et al. Improving retinal artery and vein classification by means of a minimal path approach. *Mach Vis Appl*. 2013;24:919-930.
57. Aguilar W, Martinez-Perez ME, Frauel Y, Escolano F, Lozano MA, Espinosa-Romero A. Graph-based methods for retinal mosaicing and vascular characterization. *Lecture Notes in Computer Science*. 2007;4538:25.
58. Chrástek R, Wolf M, Donath K, Niemann H, Michelson G. Automated calculation of retinal arteriovenous ratio for detection and monitoring of cerebrovascular disease based on assessment of morphological changes of retinal vascular system. *MVA*. 2002:240-243.
59. Rothaus K, Jiang X, Rhiem P. Separation of the retinal vascular graph in arteries and veins based upon structural knowledge. *Image Vis Comput*. 2009;27:864-875.
60. Gao X, Bharath A, Stanton A, Hughes A, Chapman N, Thom S. A method of vessel tracking for vessel diameter measurement on retinal images. In: *Image Processing, 2001 Proceedings 2001 International Conference of the IEEE*. 2001:881-884.
61. Narasimha-Iyer H, Beach JM, Khoobehi B, Roysam B. Automatic identification of retinal arteries and veins from dual-wavelength images using structural and functional features. *IEEE Trans Biomed Engin*. 2007;54:1427-1435.
62. Roberts DA. Analysis of vessel absorption profiles in retinal oximetry. *Med Physics*. 1987;14:124-130.
63. Joshi VS, Garvin MK, Reinhardt JM, Abramoff MD. Automated artery-vein classification of retinal blood vessels based on structural mapping method. *Proc SPIE*. 2012:8315:83151C.
64. Relan D, MacGillivray T, Ballerini L, Trucco E. Retinal vessel classification: sorting arteries and veins. In: *Engineering in*

Medicine and Biology Society (EMBC), 2013 35th Annual International Conference of the IEEE. 2013:7396-7399.

65. Vázquez S, Cancela B, Barreira N, Penedo MG, Saez M. On the automatic computation of the arterio-venous ratio in retinal

images: using minimal paths for the artery/vein classification. In: *Digital Image Computing: Techniques and Applications (DICTA), 2010 International Conference of the IEEE. 2010: 599-604.*